

NeRFmentation: NeRF-based Augmentation for Monocular Depth Estimation

Casimir Feldmann^{*,1}, Niall Siegenheim^{*,1}, Nikolas Hars¹, Lovro Rabuzin¹, Mert Ertugrul¹,
Luca Wolfart¹, Marc Pollefeys^{1,2}, Zuria Bauer^{1,3}, Martin R. Oswald^{1,4}

¹ETH Zürich, ²Microsoft, ³University of Alicante, ⁴University of Amsterdam

{cfeldmann, sniall, nihars, mertugrul, lrabuzin, wolfart1, pomarc, zbauer, moswald}@ethz.ch

Abstract

The capabilities of monocular depth estimation (MDE) models are limited by the availability of sufficient and diverse datasets. In the case of MDE models for autonomous driving, this issue is exacerbated by the linearity of the captured data trajectories. We propose a NeRF-based data augmentation pipeline to introduce synthetic data with more diverse viewing directions into training datasets and demonstrate the benefits of our approach to model performance and robustness. Our data augmentation pipeline, which we call “NeRFmentation”, trains NeRFs on each scene in the dataset, filters out subpar NeRFs based on relevant metrics, and uses them to generate synthetic RGB-D images captured from new viewing directions. In this work, we apply our technique in conjunction with three state-of-the-art MDE architectures on the popular autonomous driving dataset, KITTI, augmenting its training set of the Eigen split. We evaluate the resulting performance gain on the original test set, a separate popular driving set, and our own synthetic test set.

1. Introduction

As the field of computer vision continues to advance at a rapid pace, the pursuit of safer and more reliable autonomous driving systems remains paramount. Within this context, monocular depth estimation (MDE) plays an important role, offering a key solution to the complex challenge of depth perception in dynamic road environments. Although it offers a solution to these particular situations, it comes with extra challenges compared to stereo or in general multi-camera depth estimation. Accurately estimating the depth from a single image remains a challenging problem due to the inherent scale ambiguity in 2D projections of 3D scenes, which leads to an infinite number of geometrically plausible 3D reprojections for every 2D image.



Figure 1. **NeRFmentation.** We develop a novel dataset augmentation pipeline that utilizes NeRF-generated data rendered from poses unseen in the original dataset to improve the robustness of Monocular Depth Estimation networks. The method is intended to improve generalization capability in cases where the initial dataset provides limited spatial variability. The RGB image is taken from Waymo Open Dataset [35]

This means that monocular depth estimation is an underdetermined problem that relies on extracting and interpreting visual cues in images correctly. To address this challenge, numerous approaches leverage large-scale datasets to train deep neural networks, allowing them to learn to interpret visual cues and transform them into complex mappings between image features and corresponding depth information.

This mapping is implicitly learned from the data that is being fed into the system during training time and a common approach to making the model learn these mappings is to implement sophisticated modules to extend the underlying neural network architecture.

While improving the model architecture is a promising approach to this problem, it also introduces the need for more training data due to an increased model complexity. This need for more training data can be dealt with by adding an existing dataset or by recording a new one. The former is

^{*}Authors contributed equally

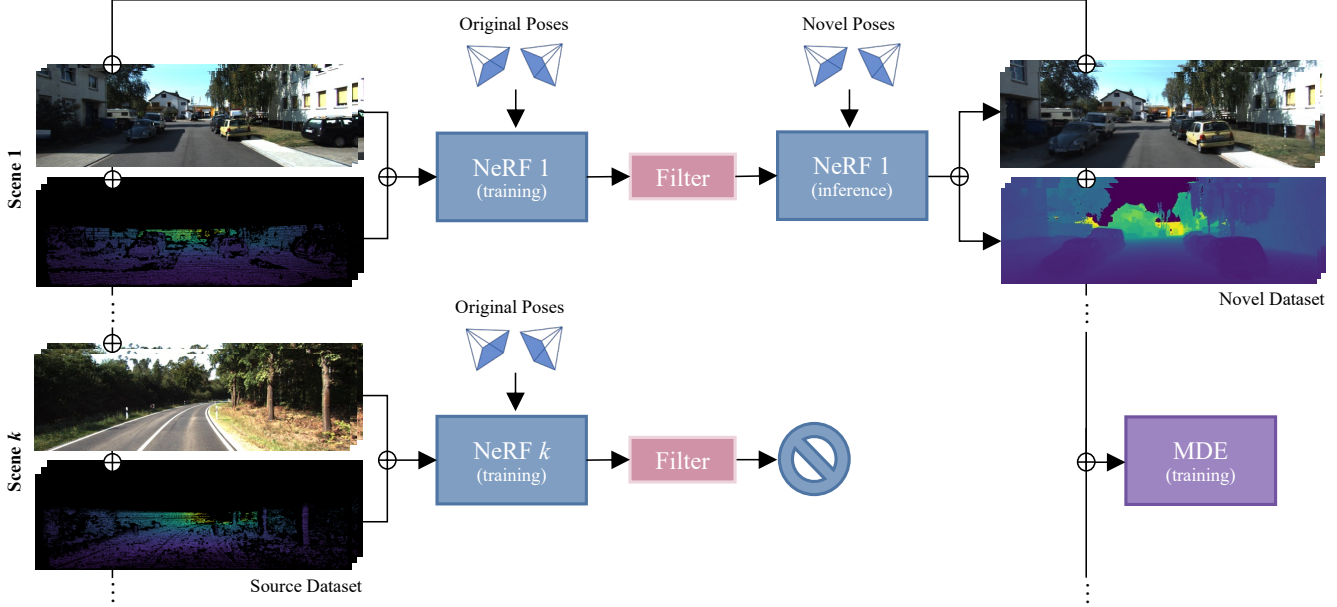


Figure 2. **Overview of our proposed pipeline.** The pipeline consists of four distinct stages. We train a NeRF for each scene in the MDE training dataset, reserving a portion of the images and poses per scene to evaluate NeRF reconstruction quality. Subpar scene NeRFs are filtered out. Then, we render novel views of the scene by systematically perturbing the original poses and querying the NeRF with these poses. Lastly, we combine the novel views with the original views of the scene to create a NeRFmented training dataset for the MDE network. Here, the source dataset is KITTI. [12]

common practice [22], although there are only finitely many real-world datasets. Recording a new dataset, however, is in the majority of cases infeasible since this introduces massive costs. This infeasibility of recording new datasets and the limited availability of real-world datasets leads to the need for different data sources. For that, one can resort to using synthetic datasets [21, 23, 26, 30]. This could lead to an unwanted domain shift which in turn can be compensated by using techniques from domain adaptation [11, 25, 39] to modify the data to match the training distribution. Domain adaptation by itself brings its own limitations as there is no guarantee that it matches the target distribution.

In recent years, however, Neural Radiance Field (NeRF) methods that can encode complete 3D scenes have emerged. These NeRFs have the ability to generate photorealistic and geometrically consistent, dense RGB-D images from novel viewpoints with remarkable accuracy.

We propose to use the capabilities of NeRFs to generate high-quality RGB-D images from novel viewpoints in order to enlarge and diversify existing real-world datasets. This method is able to match the appearance distribution of the source dataset while generating novel viewpoints that would be arduous and costly to capture by recording a new dataset. Thus, we alleviate the need for combining synthetic datasets and domain adaptation as well as making MDE models more robust to images taken from out-of-distribution poses.

These benefits come with the extra advantage that the

rendering of novel views can be automated and is very fast, while only relying upon reasonable computing power which is needed to train MDE networks anyway.

Moreover, this approach does not require designing a new model architecture, as we show that our method makes existing MDE network architectures more robust while keeping comparable performance or improving slightly with respect to the baseline.

Our main contributions are as follows:

- We propose a novel dataset augmentation scheme for Monocular Depth Estimation that leverages NeRFs to augment a limited-scale dataset via scene reconstruction and virtual view RGB-D image generation for supervised training of data-driven MDE networks.
- We conduct extensive experiments on multiple outdoor datasets, showing its robust performance gains on the target dataset, while keeping comparable performance on the source dataset which validates the effectiveness of our approach, showcasing the benefits of our scheme to MDE networks.

2. Related work

Monocular Depth Estimation. The task of Monocular Depth Estimation (MDE) involves predicting the depth values for each pixel given a monocular 2D image. Due to the inherent difficulty in predicting the correct 3D reprojection to a 2D image, well-performing models employ so-

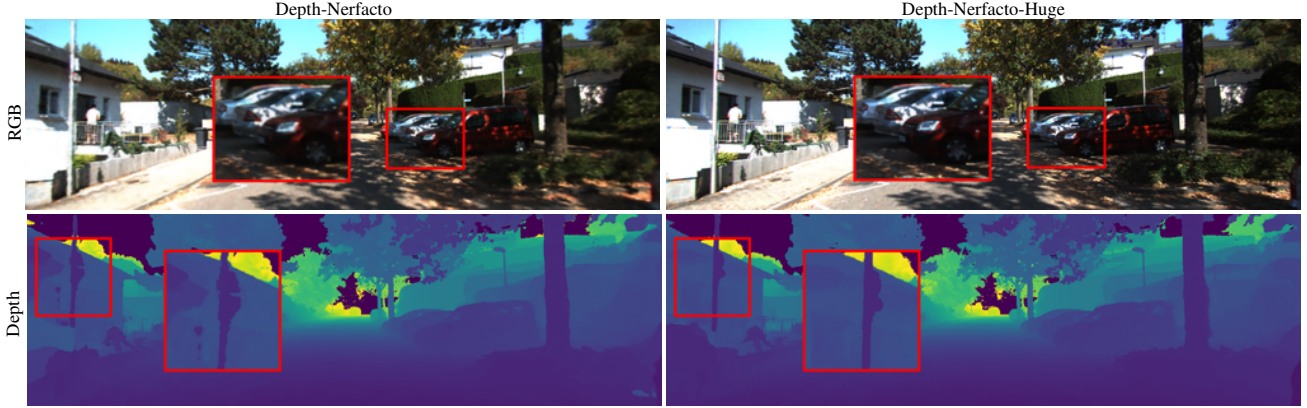


Figure 3. **Qualitative comparison of Depth-Nerfacto vs. Depth-Nerfacto-Huge reconstruction on KITTI [12].** The figure shows reconstructions of training images using both Depth-Nerfacto and Depth-Nerfacto-Huge. Depth-Nerfacto-Huge outputs exhibit higher levels of detail and better accuracy in both the generated RGB and depth images compared to Depth-Nerfacto.

phisticated data-driven methods to infer the depth values. Initially, CNN-based encoder-decoder architectures [9, 24] that interpreted the MDE task as a pure regression task were employed. With the introduction of transformers [38] and their subsequent introduction into Computer Vision as vision transformers (ViT) [8], methods that employed a combination of CNNs and ViTs emerged, such as [6, 15, 16]. AdaBins [6] is a popular example of this class of models which interprets MDE as an ordinal regression problem similar to [10] but with the addition of learning adaptive bin centers and sizes. For this, it includes a ViT [8] into the CNN itself. In contrast to AdaBins [6], DepthFormer [16] treats MDE as a pure regression problem and employs the ViT [8] to directly encode images, purportedly exploiting the ViT’s strengths. Additionally, Li *et al.* introduce the hierarchical aggregation and heterogeneous interaction (HAHI) module, to enhance ViT features and leverage the affinity between ViT and convolution features [16]. BinsFormer [15] follows the idea of combining ordinal regression on binned depth and transformer networks. We do not develop a novel MDE architecture, but instead, use AdaBins [6], DepthFormer [16], and BinsFormer [15] to show the transferability and versatility of our method.

Neural Radiance Fields (NeRFs). NeRFs are a scene representation method introduced in the seminal work [18] by Mildenhall *et al.* Using a sparse set of input views, they optimize an underlying volumetric scene function, taking advantage of a differentiable rendering pipeline. Novel views as well as depth data can then be synthesized by querying the network with novel camera poses. Nerfstudio [37] is a framework that facilitates the design, training, and testing of a wide variety of NeRF-based architectures through a modular approach. Nerfacto is an ex-

tension of the original NeRF developed by the Nerfstudio team. This model leverages the modularity of Nerfstudio to introduce new features proposed in recent NeRF literature such as camera pose refinement, per-image appearance conditioning, proposal sampling, scene contraction, and hash encoding. This combination of features leads Nerfacto to achieve near-SOTA novel view quality at a significantly faster speed than competitors such as MipNeRF [3]. Among further extensions of Nerfacto is depth-Nerfacto, extending this model with depth supervision, by providing a new loss term as proposed by Deng *et al.* [7]. Finally, Nerfacto-huge is the largest in a series of Nerfacto models offering different variants with different model sizes and capacities, offering the highest fidelity scene representations among all Nerfacto variants. When choosing an appropriate NeRF variant in our work, we once again leverage the modularity and customizability exposed by Nerfstudio to combine the aforementioned extensions of Nerfacto to benefit from both their advantages.

In the spirit of using NeRFs not only for novel view synthesis of RGBs but also other properties, MuViNeRF [42] extends Neural Radiance Fields to surface normal prediction, shading estimation, edges detection, keypoints detection, and semantic labeling. The authors argue that exploiting the pose data for predictions leads to better results than when using traditional CNNs.

Data augmentation. Data augmentation is a well-established regularization technique in Machine Learning that generally enables the training of increasingly complex models by applying software-based label-preserving transforms to scarce data. These augmentations for Convolutional Neural Networks (CNNs) and derived models started off with simple transformations such as random transla-

Method	$\delta_1 \uparrow$	$\delta_2 \uparrow$	$\delta_3 \uparrow$	REL \downarrow	SQ. REL \downarrow	RMS \downarrow	RMS LOG \downarrow
AdaBins	0.561	0.851	0.933	0.224	2.201	8.027	0.328
+Reconstructed	0.658	0.879	0.944	<u>0.204</u>	2.056	<u>7.397</u>	<u>0.292</u>
+Interpolated	0.681	<u>0.874</u>	<u>0.940</u>	0.200	<u>2.156</u>	7.389	0.286
+Angled $\pm 3^\circ$	0.632	0.855	0.929	0.215	2.237	7.835	0.313
DepthFormer	0.545	0.885	0.958	0.230	1.920	7.776	0.313
+Reconstructed	<u>0.607</u>	0.907	0.969	<u>0.199</u>	1.723	7.730	0.275
+Interpolated	0.669	0.926	0.975	0.184	1.542	6.755	0.252
+Angled $\pm 3^\circ$	0.602	<u>0.909</u>	<u>0.970</u>	<u>0.199</u>	<u>1.711</u>	<u>7.286</u>	<u>0.274</u>
BinsFormer	0.571	0.901	0.966	0.208	1.782	7.547	0.289
+Reconstructed	<u>0.702</u>	0.924	<u>0.973</u>	<u>0.183</u>	1.598	<u>6.714</u>	<u>0.249</u>
+Interpolated	0.707	0.928	0.975	0.181	1.556	6.563	0.244
+Angled $\pm 3^\circ$	0.680	<u>0.925</u>	0.975	0.185	<u>1.573</u>	6.866	0.251

Table 1. **AdaBins, DepthFormer, and BinsFormer trained on augmented KITTI dataset evaluated on the Waymo dataset.** We showcase the performance of AdaBins [6], DepthFormer [16], and BinsFormer [15] models trained on the KITTI Eigen [9, 12] train split and compare it to the NeRFmented (Ours) versions of the same models evaluated against the unseen Waymo Open Dataset. Our method greatly increases the robustness to unseen data, as demonstrated by the increased performance of NeRFmented models on the Waymo dataset in comparison to the baseline models which were trained without introducing novel views. The best results are in **bold** dark green. Second best results are underlined light green.

tions, rotations, or flips [13, 32]. Recent advancements in generative modeling have enabled the creation of photo-realistic synthetic data through increasingly sophisticated data augmentation techniques. These methods are based on Generative Adversarial Networks (GANs) [5, 27] or diffusion models [1, 2]. Sandfort *et al.* employ CycleGAN [43], a GAN that enforces cycle-consistency, to augment images for medical CT segmentation tasks [27] and successfully improve the performance even for out-of-distribution samples. While Rajpal *et al.* show in [21] that it is possible to improve monocular depth estimation performance on real-world data using a fully synthetic custom dataset, we aim to show that real-world datasets can be extended synthetically using NeRFs to improve the performance. Yen-Chen *et al.* [40] use NeRFs for robotic action planning by building a 3D scene representation and subsequently using novel view synthesis of orthographic images. The authors are able to show that compared to images produced by physical cameras, these synthetic orthographic images allow for better pixel-wise action values correlated with picking and placing success of objects by the robot.

Mancini *et al.* [17] argue for the need for generalization of MDE networks for autonomous mobile robots, to “guarantee robust operation in real-world scenarios”. To achieve this, they train on two synthetic datasets, one urban environment and one forest environment. They then test the models trained on the synthetic datasets on KITTI, where they achieve results comparable to Eigen *et al.* [9]. They also test on two datasets they collected themselves to test generalization, one is of countryside roads, and one is of a forest. They find that the network trained on both urban and

forest environments performs better than networks trained only on one of the scenarios.

Bauer *et al.* [4] use novel view synthesis to improve depth prediction. They use three blocks: one network to predict depth, a block that transforms views from one direction to another, by using the available depth data, and one network which reconstructs the image obtained from the previous block, since it is imperfect. They manage to beat the state of the art in one metric on the KITTI dataset.

3. Methods

We propose a dataset augmentation technique for Monocular Depth Estimation which is, to the best of our knowledge, novel. We leverage the fact that many real-world image datasets have a sequence-like structure, meaning that the same environment is captured from many slightly different viewpoints. Furthermore, pose data for each frame is often either provided or can be inferred through structure-from-motion, for example using COLMAP [28, 29]. Using this data, we train NeRFs to encode 3D scenes and subsequently render novel RGB-D images from unobserved poses.

We apply our proposed augmentation method to the KITTI Eigen training split [9, 12] and create a “NeRFmented” version of it to show the diversity of scenes to which our method can be applied. We train the off-the-shelf MDE models AdaBins [6], DepthFormer [16], and BinsFormer [15] on the NeRFmented dataset and evaluate them on the original dataset against their vanilla-trained model to show the transferability between different architectures. Finally, we evaluate the NeRFmented models vs the vanilla-trained models on a different dataset that the models have

not seen during training to show the added robustness and diversity that our method introduces. The ablation dataset is the Waymo Open Dataset [35].

3.1. Proposed pipeline

For each scene in the source dataset, we train a separate NeRF using RGB-D images and their corresponding poses to encode a 3D representation. To ensure a high reconstruction quality for each NeRF, we withhold a small part of the input data from the training. Once the training has concluded, we use the withheld data as a small validation split to potentially filter out scenes with subpar image- or depth reconstruction quality. We use the retained NeRFs to subsequently render RGB-D images from novel viewpoints, which are typically obtained by perturbing the original poses either through translation or rotation. Finally, we combine the RGB-D images from our novel views with the source dataset to form an augmented dataset and train the downstream monocular depth estimation network on it. The overall pipeline is depicted in Figure 2.

3.2. Scene representation model

For the NeRFs of our pipeline we use the off-the-shelf Nerfstudio framework [37], which provides convenient access to various NeRF extensions. Because our method requires high-quality depth reconstruction and image reconstruction, we base our model on a combination of the depth-Nerfacto and Nerfacto-huge architectures, which were both introduced by Tancik *et al.* in [37]. This way, we benefit from depth-supervision that is included in the depth-Nerfacto training while increasing the learning capacity of the network by replacing the MLP of depth-Nerfacto with the larger MLP of Nerfacto-huge. Figure 3 shows the qualitative performance gain of our depth-Nerfacto-huge compared to the vanilla depth-Nerfacto. We implement a filtering step which eliminates NeRFs that fail to meet a specified dataset-dependent reconstruction quality standard. To achieve this, we utilize the trained NeRF for each scene to render the RGB-D images from the poses of the small withheld validation split and compare them to the corresponding ground-truth RGB-D images. This involves computing the absolute relative error to assess the depth reconstruction quality and the LPIPS score [41] to evaluate the image reconstruction quality. We define dataset-specific thresholds for both metrics and any NeRF that falls below these thresholds is discarded.

4. Experiments

4.1. Datasets

KITTI [12]. The KITTI dataset is an outdoor dataset designed for diverse autonomous driving scenarios, featuring stereo-image pairs and annotated LiDAR ground-truth

depth data. The KITTI Eigen split [9] is a popular split of the dataset for monocular depth estimation with approximately 23,000 stereo-image pairs for training which are separated into 32 scenes for training and validation. The corresponding validation split consists of 888 stereo-image pairs. The test split contains 697 images from 29 different scenes.

Waymo Open Dataset [35]. The Waymo Open Dataset (Waymo) dataset is a large-scale outdoor dataset collected and developed by Waymo LLC for various autonomous driving tasks. The dataset incorporates data from five high-resolution pinhole cameras and five LiDARs and other sensors, which offers a wider range of camera viewpoints, denser depth maps, and a more thorough overview of the surroundings compared to datasets such as KITTI [12]. This enables more robust training of models used for autonomous driving tasks. To evaluate the robustness of our NeRFmented models, we test them against the Waymo test dataset. We choose to use only the subset of the test set coming from the front, front-left, and front-right facing cameras. We do this to avoid too large of a domain shift from the standard MDE datasets based on images taken by forward-facing cameras, such as KITTI.

4.2. Monocular Depth Estimation models

To show that our augmentation technique is model-agnostic, we show it in combination with three popular MDE models: AdaBins [6], DepthFormer [16], and BinsFormer [15]. We train and evaluate using the Monocular-Depth-Estimation-Toolbox [14], an open-source monocular depth estimation toolbox aimed at collecting several state-of-the-art MDE models into a single environment. Due to computational constraints, we can not use the original batch size used for DepthFormer and BinsFormer. Hence, we decrease the learning rate and increase the number of iterations accordingly.

For the evaluation of the MDE models, we use the same metrics as in [4]. For their definitions we refer to the supplementary material.

4.3. Training of NeRFs

We train our depth-Nerfacto-huge model on each scene of the KITTI Eigen [9, 12] train split and retain 10 % of the training data as a validation split. As we experimentally find that the reconstruction quality of NeRFs drastically reduces as the size of a scene increases, the varying size of the scenes in the KITTI dataset requires splitting them into sub-scenes. We do not want to decrease the scene size too much though, as this would increase the computational complexity and bring no additional gain when rendering novel views from challenging poses. In our case, we ensure that no pose in each sub-scene should be more than 50m away from the

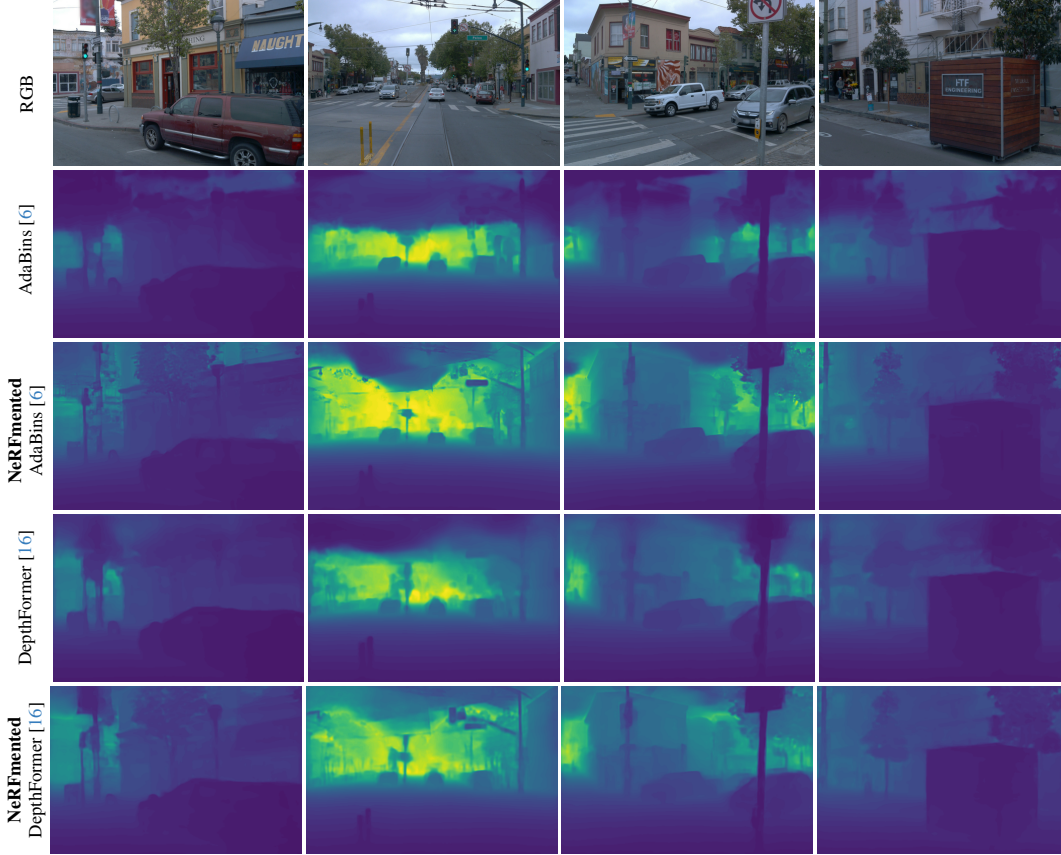


Figure 4. **Qualitative Results on the Waymo [36] dataset.** We show the performance of NeRFmentation (Ours) compared to vanilla-trained AdaBins [6] and DepthFormer [16] leading to improved predictions by using NeRF augmented data for introducing additional viewpoints in the training images. Both the NeRFmented models and vanilla-trained models have been trained on the KITTI Eigen [9, 12] train split and evaluated on the unseen Waymo Open Dataset. Color scale: 0 (purple) to 80 meters (yellow).

first pose in that sub-scene to solve the mentioned trade-off. For each sub-scene, we train a separate NeRF.

For each NeRF, we tune the weight of the depth loss and whether the poses are refined or not by running a grid search for 10,000 steps. We observe that when using NeRFs for 3D reconstruction, there is a strong trade-off between RGB quality and accuracy of the geometry, which in turn affects the accuracy of the depth maps. Since we require both to be of high quality, we use the small validation split that we withheld from the training and re-render the RGB-D images for each of their poses using all NeRFs from our grid search. Then, we select the NeRF that minimizes a trade-off validation measure

$$T_{\text{RGBD}} = \sqrt{\alpha \cdot \text{Abs. Rel}^2 + \text{LPIPS}^2} \quad (1)$$

where we use the absolute relative error of the reprojected depth maps as a quality measure of the geometry and the LPIPS score [41] as a quality measure of the RGB reconstruction. We set $\alpha = 10$ for this experiment.

Finally, we continue training the best run of the hyper-

parameter tuning of each NeRF until we reach 30,000 iterations. Then, we apply the filtering step described in Section 3.2 using the same validation split where we discard all sub-scenes and their corresponding NeRF, where the NeRF did not achieve an LPIPS score of less than 0.22 or an absolute relative error of less than 0.05 on the 3D reconstructions. We choose the threshold for LPIPS empirically by observing which value produces minimally visually acceptable RGB images. The threshold for depth absolute relative error is chosen because it is an approximate lower bound of state-of-the-art MDE networks. We filter any scenes with a higher score so as not to introduce extraneous noise into the training dataset.

Figure 6 shows the images reconstructed by NeRFs alongside ground-truth images present in the KITTI dataset. Apart from a low LPIPS score, visual inspection of the reconstructed RGB images also suggests that they are of comparable quality to the original. Additionally, the reconstructed depth maps are dense, whereas the ground-truth ones are sparse. The low absolute relative error of the re-

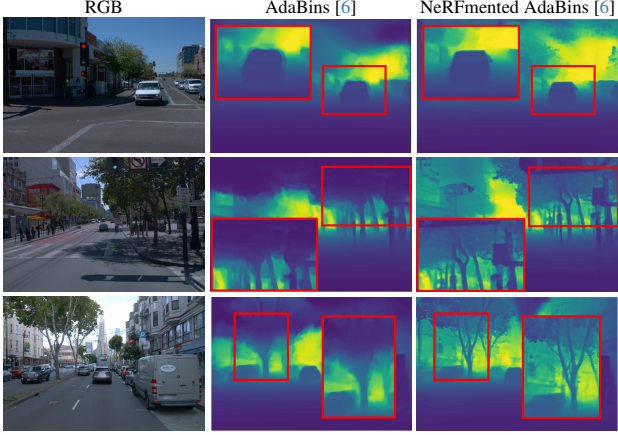


Figure 5. **Qualitative results on the Waymo [36] dataset, focusing on close-up details.** We show the qualitative close-ups of the performance of the vanilla-trained AdaBins [6] vs our proposed NeRFmented AdaBins, demonstrating the capability of our method to recover fine grain details in the prediction that the baseline is not able to predict. Color scale: 0 (purple) to 80 meters (yellow).

constructed depth maps indicates a high agreement between the original and reconstructed depth maps as well.

4.4. Novel view synthesis

We propose and evaluate three data augmentation strategies: (i) **Reconstruction**: Re-rendering the exact train poses used to train the NeRF. This completes the sparse depth from the source dataset. (ii) **Interpolated**: Creating novel poses by interpolating between pairs of training poses as these poses inject additional data while benefiting from good depth and RGB supervision. (iii) **Angled**: Rendering two additional views for each train pose, rotated $\pm 3^\circ$ horizontally as this injects the most diverse data while simulating a plausible motion performed by a driving car. For the KITTI Eigen train split [9, 12] this results in dataset sizes of (i) 29,836 (+28%), (ii) 29,744 (+28%), and (iii) 32,132 images (+39%).

The motivation behind these data augmentation strategies is to evaluate whether it is sufficient to use NeRFs as depth completion networks or whether certain novel views of training scenes can improve performance on evaluation datasets.

4.5. Training on KITTI

We train the described off-the-shelf MDE networks on the original KITTI Eigen [9, 12] train split and on our NeRFmented version of it and compare the results based on the standard MDE metrics. Our models are trained from scratch using the same hyper-parameters as described in the corresponding papers to show the influence of our augmentation method compared to the baseline without additional factors contributing to the performance change.

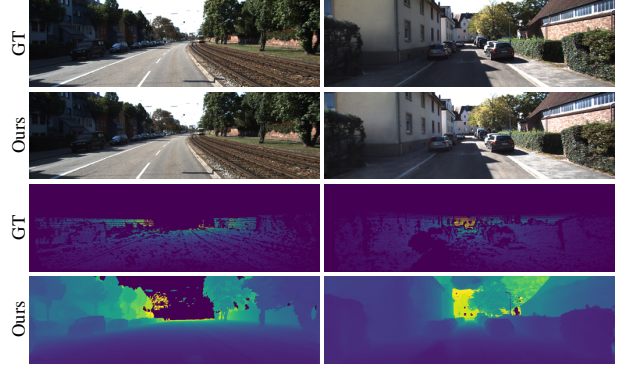


Figure 6. **Qualitative NeRF reconstruction results on KITTI [12].** We show original images from the KITTI dataset and the corresponding images generated using the trained and filtered NeRFs for the same camera poses. It is evident that reconstructed RGB images are very close to their real counterparts. The NeRFs also complete the sparse ground truth depth maps.

Augmentation	δ_1	δ_2	δ_3	REL	SQ. REL	RMS	RMS _{log}
	\uparrow	\uparrow	\uparrow	\downarrow	\downarrow	\downarrow	\downarrow
AdaBins	0.964	0.995	0.999	0.058	0.190	2.360	0.088
+Reconstructed	<u>0.961</u>	0.995	0.999	<u>0.060</u>	<u>0.204</u>	2.434	<u>0.092</u>
+Interpolated	0.960	0.995	0.999	0.61	<u>0.204</u>	<u>2.408</u>	<u>0.092</u>
+Angled $\pm 3^\circ$	<u>0.961</u>	0.995	0.999	0.061	<u>0.204</u>	2.412	0.093
DepthFormer	<u>0.975</u>	0.997	0.999	<u>0.052</u>	0.158	2.143	<u>0.079</u>
+Reconstructed	0.974	0.997	0.999	<u>0.052</u>	<u>0.152</u>	<u>2.109</u>	0.098
+Interpolated	0.976	0.997	0.999	<u>0.052</u>	0.150	2.072	<u>0.079</u>
+Angled $\pm 3^\circ$	0.974	0.997	0.999	0.051	0.150	2.072	0.078
BinsFormer	0.974	0.997	0.999	0.052	0.151	2.098	0.079
+Reconstructed	0.974	0.997	0.999	<u>0.054</u>	<u>0.155</u>	<u>2.104</u>	<u>0.081</u>
+Interpolated	<u>0.973</u>	0.997	0.999	0.055	0.157	2.125	<u>0.081</u>
+Angled $\pm 3^\circ$	<u>0.973</u>	0.997	0.999	0.055	0.159	2.164	0.082

Table 2. **Comparison of performances on the KITTI Eigen [9, 12] test split.** We showcase the performance of AdaBins [6], DepthFormer [16] and BinsFormer [15] models trained on the KITTI Eigen [9, 12] train split and compare it to the NeRFmented versions of the same models, using different novel view generation strategies. NeRFmented models stay very close to baseline performance. The best results are in **bold** dark green. The second best results are underlined light green.

Among the three MDE architectures trained with NeRFmented variants of the KITTI Eigen train split, in Table 2 we see that the DepthFormer models surpass the baseline model trained on the standard KITTI Eigen train split. The angled $\pm 3^\circ$ NeRFmentation yields an improvement in the majority of metrics we evaluate for, breaking even for the rest. The interpolated NeRFmentation is not far behind, yielding better results for 3/7 metrics while the reconstructed NeRFmentation is behind both, suggesting that the introduction of diverse poses through angle variation and interpolation introduces novel information that the MDE visibly benefits from.

4.6. Zero-shot dataset transfer to Waymo

Evaluation on a different dataset provides a good insight into generalization capabilities. In this comparison, the models are strictly trained on KITTI and KITTI-based NeRFmented images. Table 1 shows that the NeRFmented runs deliver massive uplifts across the board, beating baseline performance in a large majority of metrics for every single augmentation strategy. Notably, interpolation outperforms reconstruction and angling most of the time, likely as it strikes a good balance between providing novel viewpoints while staying close to train data distribution.

The quantitative success is mirrored by the qualitative results displayed in Figures 4 and 5. As a result of the densification of the depth maps, the MDE architecture gains supervision in the upper part of the image. This effect can be seen in the increased clarity in the upper parts of the predicted depth maps. Additionally, an increase in fine detail prediction in street signs, stoplights, street lamps, and foliage is clearly visible. Car outlines become sharper and background building details are much improved as well.

4.7. Ablation on NeRF-generated KITTI dataset

To demonstrate that NeRFmented MDE architectures generalize better on disturbed non-ideal test sets, we generate our own dataset by using novel views. More specifically, we train NeRFs on 111 sub-scenes from the KITTI Eigen test split. Then to filter out subpar scene representations, we set the LPIPS threshold to 0.3 and absolute relative error to 0.05, leaving 15 scenes for rendering. To render novel views, poses are disturbed randomly in the x and y directions and rotated randomly along each axis. This yields a test set with **1,218** dense RGB-D pairs.

In table 3 we see significant improvement in all metrics for all evaluated depth architectures using NeRFmented data. The trend of interpolation resulting in the best performance can be observed here as well.

5. Discussion

In this paper, we explore the idea of increasing the accuracy and robustness of monocular depth estimators by synthesizing new data from KITTI and introducing new views to train on. Our experiments show that for evaluation on sparse depth, we are able to achieve a performance close or better to the one when training on the vanilla dataset. For evaluation on disturbed densified depth we achieve better performance with all of the MDE networks we used as baselines. This shows that NeRFmented images are desirable if the sharpness of the depth maps is of interest. We also find that introducing new views greatly increases robustness since performance is much better when testing on an unseen dataset than without.

Augmentation	δ_1	δ_2	δ_3	REL	SQ. REL	RMS	RMS _{log}
	↑	↑	↑	↓	↓	↓	↓
AdaBins	0.761	0.961	0.988	0.183	0.987	4.248	0.211
+Reconstructed	<u>0.901</u>	0.985	0.995	<u>0.128</u>	<u>0.645</u>	<u>3.424</u>	<u>0.143</u>
+Interpolated	0.903	0.986	0.995	0.121	0.603	3.359	0.139
+Angled $\pm 3^\circ$	0.892	<u>0.983</u>	<u>0.994</u>	0.132	0.682	3.541	0.147
DepthFormer	0.791	<u>0.978</u>	<u>0.992</u>	0.171	0.840	3.804	0.193
+Reconstructed	<u>0.917</u>	0.989	0.996	<u>0.112</u>	<u>0.504</u>	3.140	0.130
+Interpolated	0.922	0.989	0.996	0.106	0.457	3.009	0.126
+Angled $\pm 3^\circ$	<u>0.917</u>	0.989	0.996	<u>0.112</u>	0.512	<u>3.098</u>	<u>0.129</u>
BinsFormer	0.807	0.979	0.992	0.168	0.831	3.743	0.189
+Reconstructed	<u>0.924</u>	0.990	0.997	<u>0.111</u>	<u>0.492</u>	<u>3.045</u>	<u>0.128</u>
+Interpolated	0.925	0.990	0.996	0.105	0.459	2.994	0.125
+Angled $\pm 3^\circ$	0.914	<u>0.988</u>	<u>0.996</u>	0.118	0.562	3.235	0.133

Table 3. **Comparison of performances on the disturbed densified KITTI dataset.** This table shows the performance of baseline and NeRFmented models evaluated on a dataset of images generated using NeRFs trained on scenes not part of the KITTI Eigen [9, 12] train split. Our method improves upon baseline performance independent of the architecture used. The best results are in **bold** dark green. The second best results are underlined light green.

Limitations. Our proposed method increases the accuracy and robustness of monocular depth estimators by remedying a lack of dense depth maps, limited viewing angles, and a general lack of scene diversity. However, given a dataset already rich with dense depth maps, varied viewing angles, and diverse scenes, NeRFmentation shows no improvement in comparison with baseline methods. The NYU-Depth V2 (NYU) dataset [31] is an example of this. It is an indoor dataset of various commercial and residential scenes captured using Microsoft Kinect. As such, the depth maps in the NYU dataset are dense. Furthermore, the dataset was recorded by manually panning the Kinect sensor. As a result, the scenes are captured from various viewpoints. We conjecture that the dense depth maps and varied poses constrain NeRFmentation’s potential for performance and robustness improvement. We provide experimental evidence for this in the supplementary material.

Future work. NeRFs are good at compressing and interpolating data. However, they lack the ability to model regions that were unobserved during training. Thus, when we render novel views where parts of the image were unobserved during the training process, no constructive prediction can be made by the NeRF. As such these parts of the image are filled with noise, unnecessarily punishing the MDE. A masking strategy based on knowledge of observed areas of the scene is delivered in the supplementary material. Dynamic objects such as cars and people are incorrectly reconstructed due to the static world assumption made. Dynamic NeRF methods such as [19, 20, 33] could remedy this shortcoming, allowing for even higher fidelity data synthesis.

Acknowledgements

One of the authors is funded by 2023/00027/001 under the “Campaign financed by the European Union Next Generation - Recovery Plan - Competent Ministry - Spanish Government”.

References

- [1] Shekoofeh Azizi, Simon Kornblith, Chitwan Saharia, Mohammad Norouzi, and David J. Fleet. Synthetic Data from Diffusion Models Improves ImageNet Classification, 2023. arXiv:2304.08466 [cs]. 4
- [2] Dmitry Baranchuk, Ivan Rubachev, Andrey Voynov, Valentin Khrulkov, and Artem Babenko. Label-Efficient Semantic Segmentation with Diffusion Models, 2022. arXiv:2112.03126 [cs]. 4
- [3] Jonathan T. Barron, Ben Mildenhall, Matthew Tancik, Peter Hedman, Ricardo Martin-Brualla, and Pratul P. Srinivasan. Mip-nerf: A multiscale representation for anti-aliasing neural radiance fields, 2021. 3
- [4] Zuria Bauer, Zuoyue Li, Sergio Orts-Escolano, Miguel Cazorla, Marc Pollefeys, and Martin R. Oswald. NVS-MonoDepth: Improving Monocular Depth Prediction with Novel View Synthesis. In *2021 International Conference on 3D Vision (3DV)*, pages 848–858, London, United Kingdom, 2021. IEEE. 4, 5, 1, 2
- [5] Victor Besnier, Himalaya Jain, Andrei Bursuc, Matthieu Cord, and Patrick Pérez. This dataset does not exist: training models from generated images, 2019. arXiv:1911.02888 [cs, eess]. 4
- [6] Shariq Farooq Bhat, Ibraheem Alhashim, and Peter Wonka. AdaBins: Depth Estimation using Adaptive Bins. In *2021 IEEE/CVF Conference on Computer Vision and Pattern Recognition (CVPR)*, pages 4008–4017, 2021. arXiv:2011.14141 [cs]. 3, 4, 5, 6, 7, 1, 2, 8
- [7] Kangle Deng, Andrew Liu, Jun-Yan Zhu, and Deva Ramanan. Depth-supervised NeRF: Fewer Views and Faster Training for Free. In *2022 IEEE/CVF Conference on Computer Vision and Pattern Recognition (CVPR)*, pages 12872–12881, New Orleans, LA, USA, 2022. IEEE. 3
- [8] Alexey Dosovitskiy, Lucas Beyer, Alexander Kolesnikov, Dirk Weissenborn, Xiaohua Zhai, Thomas Unterthiner, Mostafa Dehghani, Matthias Minderer, Georg Heigold, Sylvain Gelly, Jakob Uszkoreit, and Neil Houlsby. An image is worth 16x16 words: Transformers for image recognition at scale. In *International Conference on Learning Representations*, 2021. 3
- [9] David Eigen, Christian Puhrsch, and Rob Fergus. Depth map prediction from a single image using a multi-scale deep network, 2014. 3, 4, 5, 6, 7, 8, 1, 2
- [10] Huan Fu, Mingming Gong, Chaohui Wang, Kayhan Batmanghelich, and Dacheng Tao. Deep ordinal regression network for monocular depth estimation. *CoRR*, abs/1806.02446, 2018. 3
- [11] Leon A. Gatys, Alexander S. Ecker, and Matthias Bethge. Image style transfer using convolutional neural networks. In *Proceedings of the IEEE Conference on Computer Vision and Pattern Recognition (CVPR)*, 2016. 2
- [12] A Geiger, P Lenz, C Stiller, and R Urtasun. Vision meets robotics: The KITTI dataset. *The International Journal of Robotics Research*, 32(11):1231–1237, 2013. 2, 3, 4, 5, 6, 7, 8, 1
- [13] Alex Krizhevsky, Ilya Sutskever, and Geoffrey E Hinton. ImageNet Classification with Deep Convolutional Neural Networks. In *Advances in Neural Information Processing Systems*. Curran Associates, Inc., 2012. 4
- [14] Zhenyu Li. Monocular depth estimation toolbox. <https://github.com/zhyever/Monocular-Depth-Estimation-Toolbox>, 2022. 5
- [15] Zhenyu Li, Xuyang Wang, Xianming Liu, and Junjun Jiang. Binsformer: Revisiting adaptive bins for monocular depth estimation, 2022. 3, 4, 5, 7, 1, 8
- [16] Zhenyu Li, Zehui Chen, Xianming Liu, and Junjun Jiang. Depthformer: Exploiting long-range correlation and local information for accurate monocular depth estimation. *Machine Intelligence Research*, pages 1–18, 2023. 3, 4, 5, 6, 7, 1, 2, 8, 9
- [17] Michele Mancini, Gabriele Costante, Paolo Valigi, Thomas Ciarfuglia, Jeffrey Delmerico, and Davide Scaramuzza. Toward domain independence for learning-based monocular depth estimation. *IEEE Robotics and Automation Letters*, PP:1–1, 2017. 4
- [18] Ben Mildenhall, Pratul P. Srinivasan, Matthew Tancik, Jonathan T. Barron, Ravi Ramamoorthi, and Ren Ng. NeRF: Representing Scenes as Neural Radiance Fields for View Synthesis, 2020. arXiv:2003.08934 [cs]. 3
- [19] Sungheon Park, Minjung Son, Seokhwan Jang, Young Chun Ahn, Ji-Yeon Kim, and Nahyup Kang. Temporal interpolation is all you need for dynamic neural radiance fields, 2023. 8
- [20] Albert Pumarola, Enric Corona, Gerard Pons-Moll, and Francesc Moreno-Noguer. D-nerf: Neural radiance fields for dynamic scenes, 2020. 8
- [21] Aakash Rajpal, Noshaba Cheema, Klaus Illgner-Fehns, Philipp Slusallek, and Sunil Jaiswal. High-Resolution Synthetic RGB-D Datasets for Monocular Depth Estimation, 2023. arXiv:2305.01732 [cs]. 2, 4
- [22] René Ranftl, Katrin Lasinger, David Hafner, Konrad Schindler, and Vladlen Koltun. Towards robust monocular depth estimation: Mixing datasets for zero-shot cross-dataset transfer, 2020. 2
- [23] Stephan R. Richter, Vibhav Vineet, Stefan Roth, and Vladlen Koltun. Playing for data: Ground truth from computer games, 2016. 2
- [24] Olaf Ronneberger, Philipp Fischer, and Thomas Brox. U-net: Convolutional networks for biomedical image segmentation. In *Medical Image Computing and Computer-Assisted Intervention – MICCAI 2015*, pages 234–241, Cham, 2015. Springer International Publishing. 3
- [25] Christos Sakaridis, Dengxin Dai, and Luc Van Gool. Map-guided curriculum domain adaptation and uncertainty-aware evaluation for semantic nighttime image segmentation. *IEEE Transactions on Pattern Analysis and Machine Intelligence*, 2020. 2

- [26] Christos Sakaridis, Dengxin Dai, and Luc Van Gool. ACDC: The adverse conditions dataset with correspondences for semantic driving scene understanding. In *Proceedings of the IEEE/CVF International Conference on Computer Vision (ICCV)*, 2021. 2
- [27] Veit Sandfort, Ke Yan, Perry J. Pickhardt, and Ronald M. Summers. Data augmentation using generative adversarial networks (CycleGAN) to improve generalizability in CT segmentation tasks. *Scientific Reports*, 9(1):16884, 2019. Number: 1 Publisher: Nature Publishing Group. 4
- [28] Johannes L. Schonberger and Jan-Michael Frahm. Structure-from-Motion Revisited. In *2016 IEEE Conference on Computer Vision and Pattern Recognition (CVPR)*, pages 4104–4113, Las Vegas, NV, USA, 2016. IEEE. 4
- [29] Johannes L. Schönberger, Enliang Zheng, Jan-Michael Frahm, and Marc Pollefeys. Pixelwise View Selection for Unstructured Multi-View Stereo. In *Computer Vision – ECCV 2016*, pages 501–518, Cham, 2016. Springer International Publishing. 4
- [30] Shital Shah, Debadeepta Dey, Chris Lovett, and Ashish Kapoor. Airsim: High-fidelity visual and physical simulation for autonomous vehicles, 2017. 2
- [31] Nathan Silberman, Derek Hoiem, Pushmeet Kohli, and Rob Fergus. Indoor segmentation and support inference from rgbd images. In *Computer Vision–ECCV 2012: 12th European Conference on Computer Vision, Florence, Italy, October 7–13, 2012, Proceedings, Part V 12*, pages 746–760. Springer, 2012. 8, 1, 2, 3, 4, 5
- [32] P.Y. Simard, D. Steinkraus, and J.C. Platt. Best practices for convolutional neural networks applied to visual document analysis. In *Seventh International Conference on Document Analysis and Recognition, 2003. Proceedings.*, pages 958–963, 2003. 4
- [33] Liangchen Song, Anpei Chen, Zhong Li, Zhang Chen, Lele Chen, Junsong Yuan, Yi Xu, and Andreas Geiger. Nerf-player: A streamable dynamic scene representation with decomposed neural radiance fields, 2023. 8
- [34] Julian Straub, Thomas Whelan, Lingni Ma, Yufan Chen, Erik Wijmans, Simon Green, Jakob J. Engel, Raul Mur-Artal, Carl Ren, Shobhit Verma, Anton Clarkson, Mingfei Yan, Brian Budge, Yajie Yan, Xiaqing Pan, June Yon, Yuyang Zou, Kimberly Leon, Nigel Carter, Jesus Briales, Tyler Gillingham, Elias Mueggler, Luis Pesqueira, Manolis Savva, Dhruv Batra, Hauke M. Strasdat, Renzo De Nardi, Michael Goesele, Steven Lovegrove, and Richard Newcombe. The Replica dataset: A digital replica of indoor spaces. *arXiv preprint arXiv:1906.05797*, 2019. 2, 3
- [35] Pei Sun, Henrik Kretschmar, Xerxes Dotiwalla, Aurelien Chouard, Vijaysai Patnaik, Paul Tsui, James Guo, Yin Zhou, Yuning Chai, Benjamin Caine, Vijay Vasudevan, Wei Han, Jiquan Ngiam, Hang Zhao, Aleksei Timofeev, Scott Ettinger, Maxim Krivokon, Amy Gao, Aditya Joshi, Yu Zhang, Jonathon Shlens, Zhifeng Chen, and Dragomir Anguelov. Scalability in perception for autonomous driving: Waymo open dataset. In *Proceedings of the IEEE/CVF Conference on Computer Vision and Pattern Recognition (CVPR)*, 2020. 1, 5, 8
- [36] Pei Sun, Henrik Kretschmar, Xerxes Dotiwalla, Aurelien Chouard, Vijaysai Patnaik, Paul Tsui, James Guo, Yin Zhou, Yuning Chai, Benjamin Caine, Vijay Vasudevan, Wei Han, Jiquan Ngiam, Hang Zhao, Aleksei Timofeev, Scott Ettinger, Maxim Krivokon, Amy Gao, Aditya Joshi, Yu Zhang, Jonathon Shlens, Zhifeng Chen, and Dragomir Anguelov. Scalability in Perception for Autonomous Driving: Waymo Open Dataset. In *2020 IEEE/CVF Conference on Computer Vision and Pattern Recognition (CVPR)*, pages 2443–2451, Seattle, WA, USA, 2020. IEEE. 6, 7, 1, 9
- [37] Matthew Tancik, Ethan Weber, Evonne Ng, Ruilong Li, Brent Yi, Justin Kerr, Terrance Wang, Alexander Kristoffersen, Jake Austin, Kamyar Salahi, Abhik Ahuja, David McAllister, and Angjoo Kanazawa. Nerfstudio: A Modular Framework for Neural Radiance Field Development. In *Special Interest Group on Computer Graphics and Interactive Techniques Conference Proceedings*, pages 1–12, 2023. arXiv:2302.04264 [cs]. 3, 5, 1
- [38] Ashish Vaswani, Noam Shazeer, Niki Parmar, Jakob Uszkoreit, Llion Jones, Aidan N Gomez, Łukasz Kaiser, and Illia Polosukhin. Attention is all you need. In *Advances in Neural Information Processing Systems*. Curran Associates, Inc., 2017. 3
- [39] Yanchao Yang and Stefano Soatto. Fda: Fourier domain adaptation for semantic segmentation. In *Proceedings of the IEEE/CVF Conference on Computer Vision and Pattern Recognition (CVPR)*, 2020. 2
- [40] Lin Yen-Chen, Pete Florence, Andy Zeng, Jonathan T. Barron, Yilun Du, Wei-Chiu Ma, Anthony Simeonov, Alberto Rodriguez Garcia, and Phillip Isola. MIRA: Mental Imagery for Robotic Affordances, 2022. arXiv:2212.06088 [cs]. 4
- [41] Richard Zhang, Phillip Isola, Alexei A. Efros, Eli Shechtman, and Oliver Wang. The Unreasonable Effectiveness of Deep Features as a Perceptual Metric. In *2018 IEEE/CVF Conference on Computer Vision and Pattern Recognition*, pages 586–595, Salt Lake City, UT, 2018. IEEE. 5, 6
- [42] Shuhong Zheng, Zhipeng Bao, Martial Hebert, and Yu-Xiong Wang. Multi-task View Synthesis with Neural Radiance Fields, 2023. arXiv:2309.17450 [cs]. 3
- [43] Jun-Yan Zhu, Taesung Park, Phillip Isola, and Alexei A Efros. Unpaired image-to-image translation using cycle-consistent adversarial networks. In *Computer Vision (ICCV), 2017 IEEE International Conference on*, 2017. 4

NeRFmentation: NeRF-based Augmentation for Monocular Depth Estimation

Supplementary Material

A. Evaluation Metrics for MDE

We utilize the MDE evaluation metrics used in [4]. The metrics are defined as follows, given prediction \hat{y}_i and ground truth value y_i :

Relative Error (REL): $\frac{1}{N} \sum_{i=1}^N \frac{|y_i - \hat{y}_i|}{y_i}$

Squared Relative Error (SQ. REL): $\frac{1}{N} \sum_{i=1}^N \frac{|y_i - \hat{y}_i|^2}{y_i^2}$

Root Mean Squared Error (RMSE): $\sqrt{\frac{1}{N} \sum_{i=1}^N (y_i - \hat{y}_i)^2}$

Log RMSE: $\sqrt{\frac{1}{N} \sum_{i=1}^N (\log y_i - \log \hat{y}_i)^2}$

Threshold Accuracy (δ_j): $\max(\frac{y_i}{\hat{y}_i}, \frac{\hat{y}_i}{y_i}) = \delta < 1.25^j$

B. Qualitative comparison with state-of-the-art methods on the KITTI and Waymo dataset

Figures B.1 and B.2 provide additional qualitative results compared to the state-of-the-art methods AdaBins [6], Depthformer [16] and BinsFormer [15] on the KITTI [12] and Waymo [36] datasets. Qualitative improvements on KITTI are similar to those found on Waymo, our proposed method is able to predict increased details in objects such as trees and street signs, which can be especially noted in the top third part of the image.

C. Qualitative comparison between the Reconstructed, Interpolated, and Angled

We compare the three proposed data augmentation strategies in conjunction with DepthFormer in Figure C.1. The differences between the different NeRFmented depth predictions on the Waymo dataset show that they all perform similarly. This suggests that the depth completion offered by NeRFs is the significant driver behind the performance gains.

D. Scene mesh of NeRFs trained on KITTI

Using the built-in poisson mesh export in Nerfstudio [37] we generate a mesh of the NeRF scene. Figure D.1 shows a bird-eye's view and a front-facing view of a 50-meter KITTI sub-scene. This 3D representation allows us to verify that the NeRF depth map predictions are sound and consistent.

E. Discussion: NeRFmentation on NYU-Depth V2

Given the promising results produced using NeRFmentation on the task of MDE on outdoor scenes, investigating the efficacy of this method on MDE on indoor scenes becomes an

obvious follow-up question. The tasks of indoor and outdoor MDE have differing constraints, use cases, and available resources. The lack of diverse poses in outdoor scene trajectories, for instance, may not translate to indoor scenes. Here a trajectory may be captured by a device like the Microsoft Kinect, which is able to operate with a wide range of viewing angles and short physical distances between captured frames. This is because a Kinect is not limited by the lanes of a road or the speed of a vehicle. Thus, the inherent problems present in outdoor MDE and the resulting issue of data scarcity that NeRFmentation aims to tackle may have limited value for the indoor setting. Our following investigation applies the same experiments and procedures previously followed for the outdoor KITTI Dataset to the indoor NYU-Depth V2 Dataset. The performance of NeRFmentation is evaluated using AdaBins [6] and DepthFormer [16] models.

NYU-Depth V2 Dataset [31]. NYU-Depth V2 is an indoor dataset consisting of various commercial and residential scenes captured using Microsoft Kinect. The dataset comprises a smaller subset with dense segmentation labels and preprocessed depth as well as the much larger raw output of the Kinect sensor in the form of raw RGB, depth, and accelerometer data. The raw data is used for the purposes of our work, including a training set of approximately **120K** samples and a test set of **654** samples [9]. As the RGB and depth images are not synchronized, they are preprocessed using the toolbox provided by the dataset authors. The images are additionally center cropped as described by Eigen *et al.* [9].

E.1. Training on NYU-Depth V2

The aforementioned MDE networks are trained on the original NYU-Depth V2 train split and NeRFmented versions of it using the approach described in Section 4.5. The relevant results are provided in Table E.1. NeRFmentation appears to hinder performance for both models and all novel view synthesis strategies. Unlike in the case of KITTI, for NYU-Depth V2, the introduction of synthetic images may not improve generalization to a more diverse set of poses since the original data is not particularly lacking in pose diversity. Instead, the introduction of noisy images that reduce the data quality becomes the main factor determining the net outcome of the augmentation. Additionally, our experiments on the KITTI dataset suggest that dense supervision coming from NeRFmentation is a large factor in why NeRFmentation improves on vanilla training. With NYU-Depth V2, the

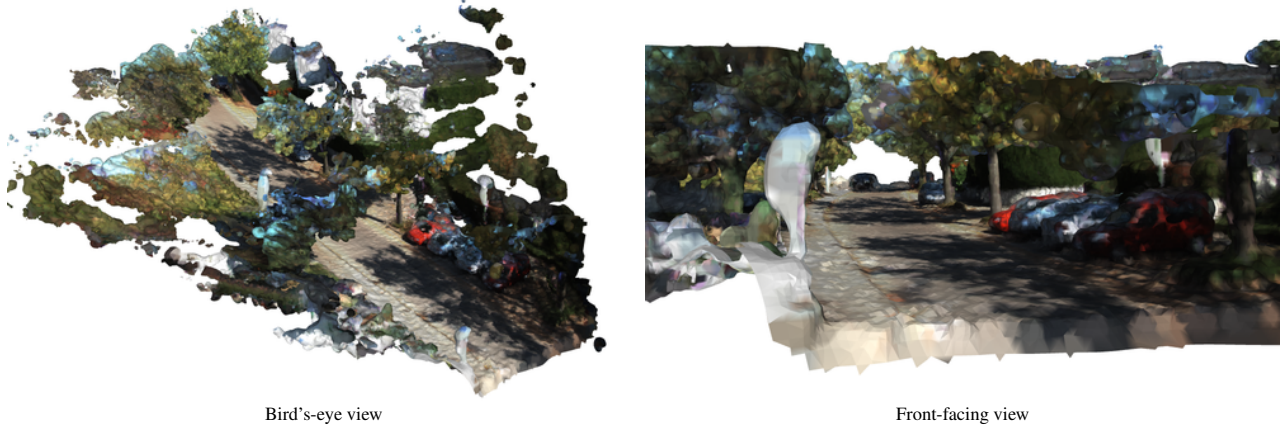


Figure D.1. **Mesh generated with NeRF that was trained on KITTI [12] sub-scene.** One can see that the underlying scene geometry is accurately learned. The bird’s-eye view shows what a single sub-scene looks like after the scene has been split into smaller 50-meter sub-scenes.

vanilla dataset already provides dense supervision. Therefore, this advantage of NeRFmentation is lost when using the NYU-Depth V2 dataset.

E.2. Zero-shot data transfer to Replica Dataset

To evaluate performance on a different indoor dataset, the Replica Dataset [34] is used. Replica consists of high-quality 3D indoor scene reconstructions, of which we choose the two validation scenes, and the one test scene from Bauer *et al.* [4] as our validation split. We modify the source code of the provided ReplicaRenderer and ReplicaViewer [34] to be able to render customized sequences of synthetic RGB-D images following a natural trajectory through each scene. NeRFmentation deteriorates generalization to the unseen data distribution of synthetic images from the Replica dataset, as seen in Table E.2 and Figure E.3. These results together with the NYU test set results show that the training data becomes too noisy for potential NeRFmentation benefits in generalization to unseen data distributions to be possible.

E.3. Ablation on NeRF-generated NYU-Depth V2 dataset

Similar to the procedure applied in the case of KITTI-based NeRFmented MDE architectures, we aim to demonstrate generalization to perturbed poses for the NYU-Depth V2 dataset. The same pose disturbance scheme as in KITTI is used, and the scheme is applied to NeRFs trained on the test scenes remaining after the same filtration process as in KITTI experiments to eliminate subpar scenes. To create a test set of approximately the same size as the original NYU-Depth V2 test set, up to 10 frames per scene are selected at equal intervals along the scene sequence, and new images are rendered using corresponding perturbed poses. With this approach, the perturbed test set consists of 700 images

covering 73 scenes, capturing a diverse set of indoor environments. As demonstrated in Table E.3, the NeRFmented MDE models surpass the baseline AdaBins [6] models in the case of NeRFmentation using reconstructed views. In contrast, the DepthFormer [16] models do not exhibit a conclusive advantage for either the NeRFmented or the vanilla-trained models.

Augmentation	δ_1 ↑	δ_2 ↑	δ_3 ↑	REL ↓	RMS ↓	\log_{10} ↓
AdaBins	0.903	0.984	0.997	0.103	0.364	0.044
+Reconstructed	0.877	0.977	0.994	0.118	0.414	0.049
+Interpolated	<u>0.898</u>	<u>0.983</u>	<u>0.996</u>	<u>0.106</u>	<u>0.375</u>	<u>0.045</u>
+Angled $\pm 3^\circ$	0.884	0.981	0.996	0.112	0.387	0.047
DepthFormer	0.921	0.989	0.998	0.096	0.339	0.041
+Reconstructed	0.909	0.987	0.997	0.101	0.350	0.043
+Interpolated	<u>0.909</u>	<u>0.987</u>	<u>0.997</u>	<u>0.101</u>	<u>0.353</u>	<u>0.043</u>
+Angled $\pm 3^\circ$	0.908	<u>0.987</u>	0.998	0.102	<u>0.350</u>	<u>0.043</u>

Table E.1. **Comparison of performances on the NYU-Depth-v2 [31] dataset.** This table shows the performance of AdaBins [6] and DepthFormer [16] models trained on the NYU-Depth V2 train split [9, 31] and compare it to the NeRFmented versions of the same models, using different novel view generation strategies. Both vanilla-trained and NeRFmented models were evaluated against the NYU-Depth V2 test split [9]. Our method yields reduced performance in most metrics for both models. The best results are in **bold** dark green. The second best results are underlined light green.

F. Future Works: Masking

Due to the sparsity of depth maps of datasets that were recorded using a LiDAR sensor such as KITTI, NeRFs that are trained on these datasets have to inter- and extrapolate

Augmentation	δ_1 ↑	δ_2 ↑	δ_3 ↑	REL ↓	RMS ↓	\log_{10} ↓
AdaBins	0.512	0.921	0.982	0.271	0.821	0.103
+Reconstructed	0.214	0.576	0.895	0.526	1.572	0.179
+Interpolated	<u>0.336</u>	<u>0.772</u>	<u>0.952</u>	<u>0.398</u>	<u>1.284</u>	<u>0.140</u>
+Angled $\pm 3^\circ$	0.300	0.713	0.916	0.418	1.297	0.157
DepthFormer	0.410	0.904	0.978	0.325	0.937	0.116
+Reconstructed	<u>0.150</u>	<u>0.606</u>	<u>0.943</u>	<u>0.526</u>	<u>1.540</u>	<u>0.175</u>
+Interpolated	0.115	0.542	0.908	0.582	1.634	0.190
+Angled $\pm 3^\circ$	0.109	0.486	0.908	0.604	1.752	0.196

Table E.2. **Comparison of performances on the Replica Dataset [34].** Models trained on the NYU-Test V2 train split [9, 31] are compared to the NeRFmented (Ours) versions of the same models evaluated against a subset of the Replica Dataset [34], a 3D scene reconstruction dataset. Our method impairs performance considerably on unseen synthetic indoor sequences, invalidating the possibility of improved generalization. The best results are in **bold** dark green. The second best results are underlined light green.

Augmentation	δ_1 ↑	δ_2 ↑	δ_3 ↑	REL ↓	RMS ↓	\log_{10} ↓
AdaBins	<u>0.706</u>	<u>0.907</u>	<u>0.960</u>	<u>0.794</u>	<u>0.750</u>	<u>0.094</u>
+Reconstructed	0.732	0.912	0.964	0.622	0.691	0.083
+Interpolated	0.315	0.804	0.939	1.235	1.159	0.147
+Angled $\pm 3^\circ$	0.311	0.804	0.936	1.347	1.129	0.148
DepthFormer	0.773	0.933	0.974	0.882	0.650	0.077
+Reconstructed	0.791	0.935	0.979	<u>0.916</u>	0.742	<u>0.074</u>
+Interpolated	0.797	<u>0.934</u>	<u>0.978</u>	0.948	<u>0.731</u>	0.072
+Angled $\pm 3^\circ$	<u>0.796</u>	0.935	0.979	0.953	0.732	0.072

Table E.3. **Comparison of performances on the perturbed NYU-Depth v2 [31] dataset.** This table shows the performance of baseline and NeRFmented models evaluated on a dataset of images generated using NeRFs trained on scenes not part of the NYU-Depth v2 train split [9, 31]. Images are generated using random disturbances to original image poses. Our method does not yield an architecture-independent performance increase, rendering the robustness ablation for indoor MDEs inconclusive. The best results are in **bold** dark green. The second best results are underlined light green.

data that they have never seen before. Interpolating data for a NeRF is mostly unproblematic. However, NeRFs struggle at the scene borders of the training data as they have to extrapolate in these regions. Due to the fact that the level of supervision approaches zero in these regions, the NeRF learns to predict noise in these regions without any guarantee that the data there is useful. In the best case, the data corresponds to the actual real-world geometry, but in the worst case, it will predict values that could hurt the overall

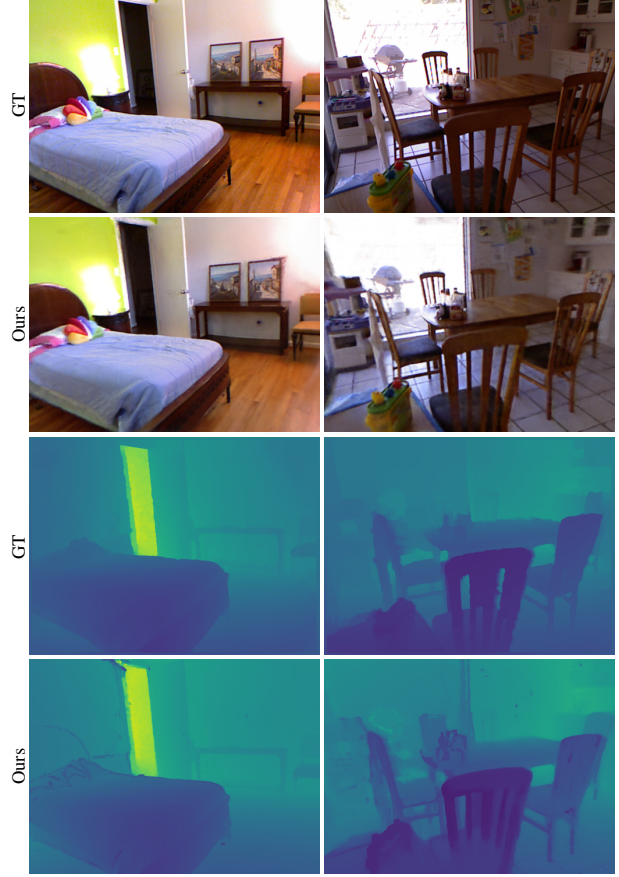


Figure E.1. **Qualitative NeRF reconstruction results on the NYU-Depth V2 Dataset [31]** We show original images from the NYU-Depth V2 dataset and the corresponding images generated using the trained and filtered NeRFs for the same camera poses. The reconstructed RGB images appear very similar to their real counterparts. The reconstructed depth maps are also very close to the ground truth depth maps. However, there is some noise apparent on the edges of objects in the reconstructed depth maps. Color scale: 0 (purple) to 10 meters (yellow).

training procedure and thus need to be taken care of. This issue limits us from rendering more diverse poses for our NeRFmentation method, as any strong rotations or extreme translations will lead to noisy, but dense renders that we cannot mask out trivially without any extra steps.

In the following, we describe our proposed method to generate non-trivial binary occupancy masks that can be used to mask out unseen regions of NeRF-rendered depth maps during the training of a MDE network. These masks are designed to prevent the network from getting penalized for predicting incorrect values in pixels corresponding to these unseen regions.

Point cloud generation. First, we need to obtain the 3D point cloud of each sub-scene s in Cartesian coordinates. For that we must first obtain the homogeneous point cloud $PC_{s,h}$ using the following Equation (2):

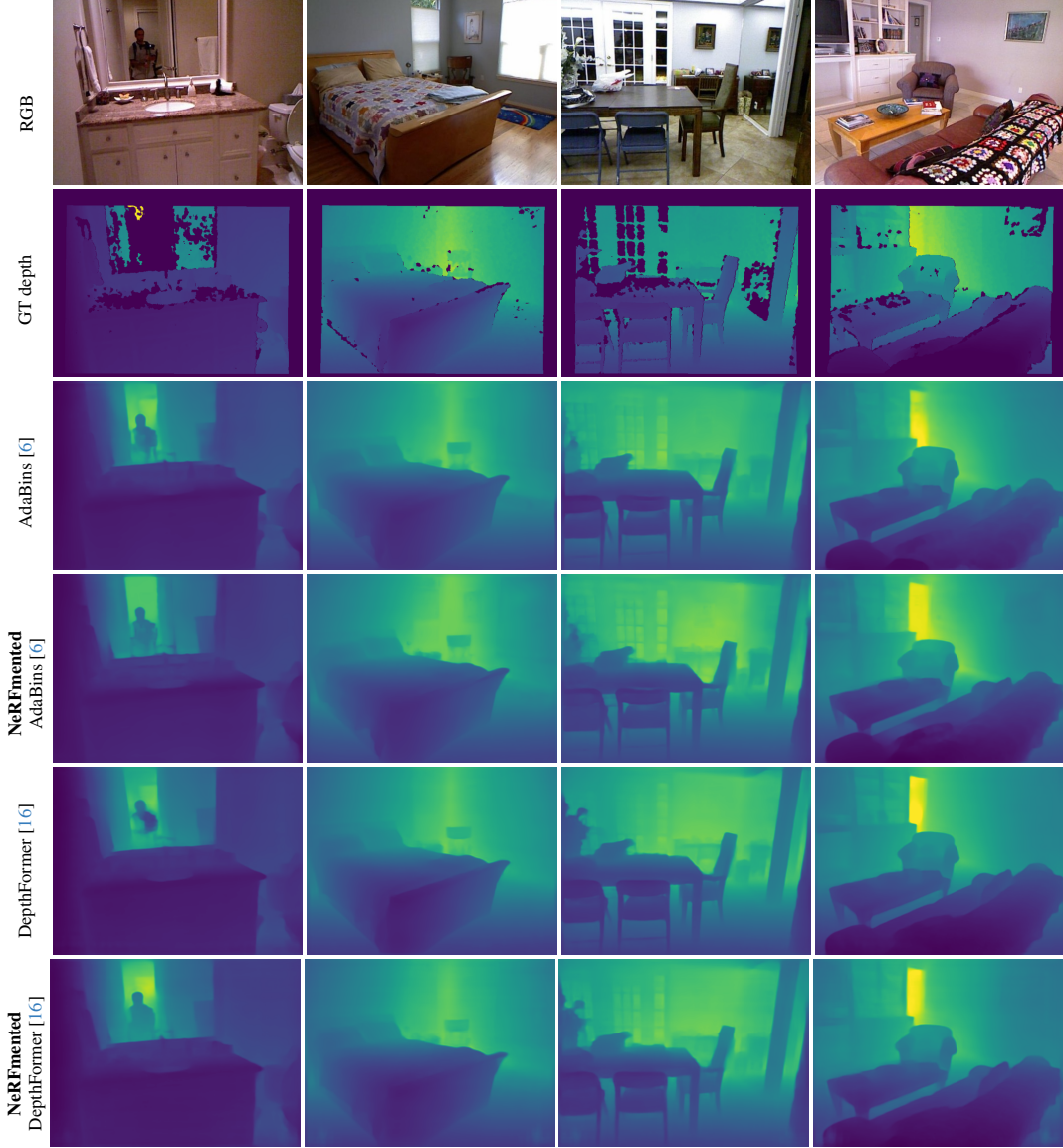


Figure E.2. **Qualitative Results on the NYU-Depth V2 Dataset [31]** We show the performance of NeRFmentation (Ours) compared to vanilla-trained AdaBins [6] and DepthFormer [16]. Both the NeRFmented models and vanilla-trained models have been trained on the NYU-Depth V2 train split and evaluated on the test split [9]. There is little discernible visual difference between the predictions of the vanilla-trained models and NeRFmented models. This is in line with the scores presented in Table E.1. Color scale: 1 (purple) to 6.5 meters (yellow).

$$\begin{aligned}
&\forall d_k \in \text{DM}_{\text{train},s} \subseteq \text{DM}_{\text{train}} \subseteq \mathcal{D}_{\text{train}}, \quad d_k \in \mathbb{R}^{U \times V}, \\
&\text{PC}_{s,h} = \{P_{W,s,h} \in \mathbb{R}^4 \mid d_k \ni d_{k,uv} > 0\}, \\
&\text{where} \\
&P_{W,s,h} = T_{C_k}^W \cdot \begin{bmatrix} (K_C^{-1} \cdot p_{k,uv})^T \cdot d_{k,uv} \\ d_{k,uv} \end{bmatrix}, \\
&K_C^{-1} \in \mathbb{R}^{3 \times 3}, \quad T_{C_k}^W \in \mathbb{R}^{4 \times 4}, \quad \text{PC}_{s,h} \in \mathbb{R}^{N \times 4}, \\
&p_{c,uk} = p_c(u, v) \in \mathbb{R}, \quad N \leq U \cdot V \cdot |\text{DM}_{\text{train},s}|.
\end{aligned} \tag{2}$$

where d_k is the k -th depth map of the training split $\text{DM}_{\text{train},s}$ of sub-scene s which is a subset of the complete training dataset $\mathcal{D}_{\text{train}}$, and $P_{W,s,h}$ is the 4-dimensional homogeneous point in the world frame. For each sub-scene s , we first unproject each valid 2D point of each sparse depth map d_k that was part of the NeRF training split $\text{DM}_{\text{train},s}$ into the camera reference frame C using homogeneous coordinates, the depth value $d_{k,uv}$ at every pixel index $u \in [0, U-1]$, $v \in [0, V-1]$ and the inverse of the given intrinsic camera matrix $K_C \in \mathbb{R}^{3 \times 3}$. Then we transform each homogeneous

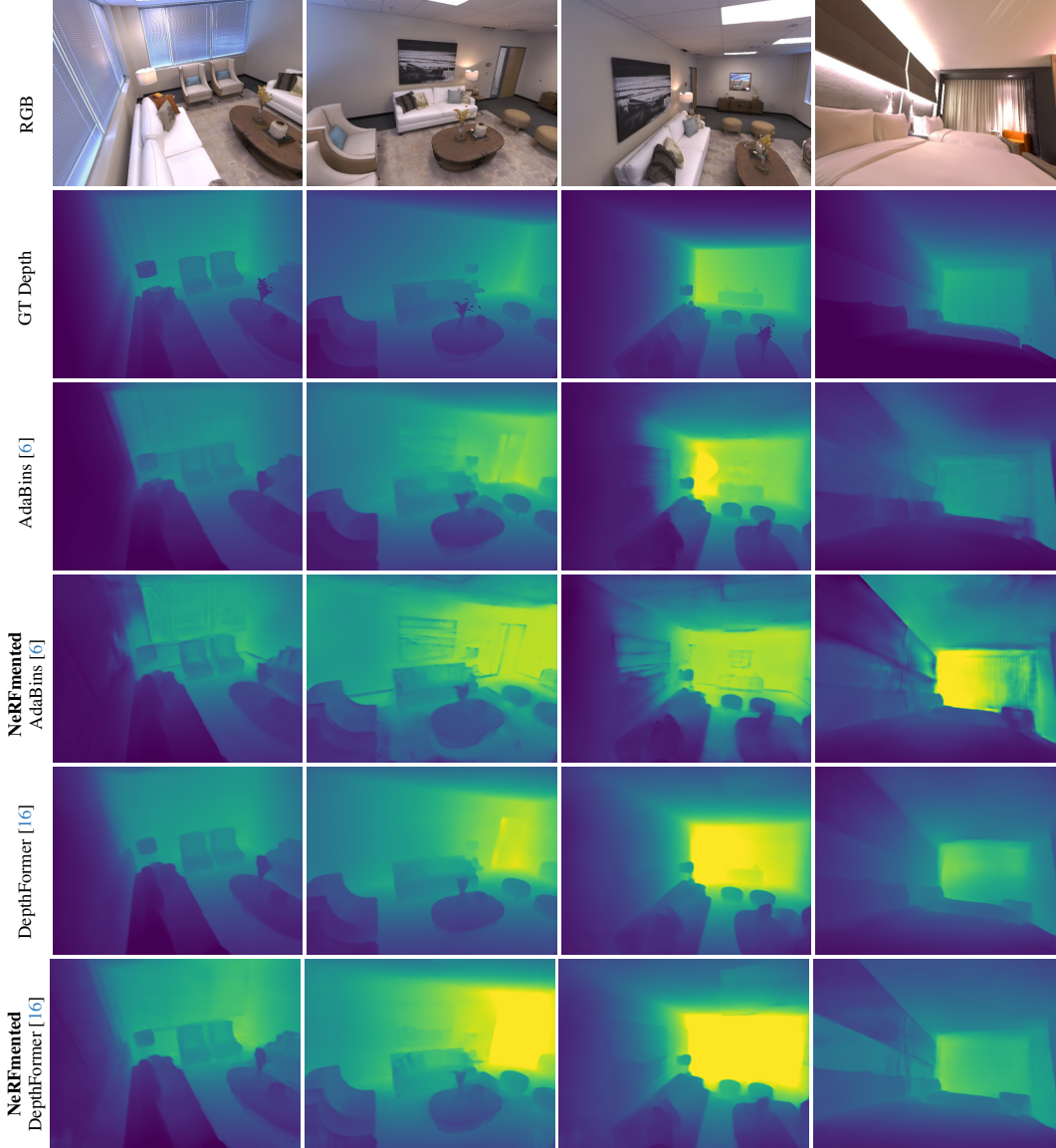


Figure E.3. **Qualitative Results on the Replica Dataset [35].** We show the performance of NeRFmentation (Ours) compared to vanilla-trained AdaBins [6] and DepthFormer [16]. Both the NeRFmented models and vanilla-trained models were trained on the NYU-Depth V2 train split [9, 31] and evaluated on a subset of the unseen Replica Dataset [35]. The NeRFmented models produce higher noise around edges of objects than the vanilla-trained models. This could be attributed to the noise introduced by NeRF-generated training data, as presented in Figure E.1. Color scale: 1 (purple) to 8 meters (yellow).

point into the world coordinate system W using the given extrinsic matrices $T_{C_k}^W \in \mathbb{R}^{4 \times 4}$. After this step, the 3D point cloud PC_s is derived by dividing each point in $PC_{s,h}$ by its fourth homogeneous coordinate

$$PC_s = \frac{1}{PC_{s,h}[3]} \cdot \begin{bmatrix} PC_{s,h}[0] \\ PC_{s,h}[1] \\ PC_{s,h}[2] \end{bmatrix}, \quad (3)$$

where $PC_{s,h}[i]$ denotes the i -th element of the homogeneous point cloud $PC_{s,h}$.

Mask generation. When we generate an RGB-D image from a novel view, we store the pose used for each RGB-D image and split it into a rotation matrix $R_W^{NV_k}$ and a translation vector $t_W^{NV_k}$ to project the point cloud into the reference frame of the novel view NV and using the intrinsic camera matrix K_C , we can then project the point-cloud into the image as a 2D projection and set the value for each pixel to 1 if it is occupied by data from at least one 3D point. This operation is the inverse of the point cloud generation process. It is described in the following equation 4:

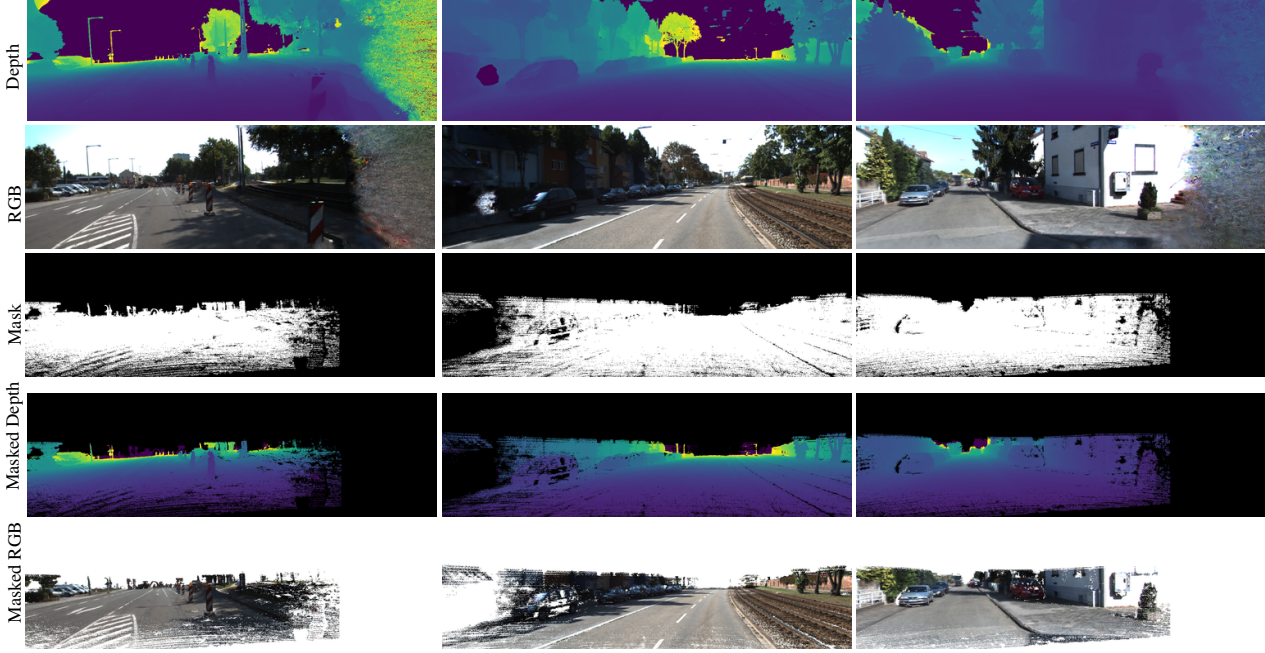


Figure F.1. **NeRF reconstruction results with 15 degrees rotation and occupancy masks on KITTI [12].** We show novel views from KITTI that were generated by rotating 15 degrees to the left or right, starting from a training pose. We show the rendered, dense depth map and the rendered RGB image which clearly show artifacts in the border regions. Using the occupancy masks, it is possible to filter out these artifacts, but at the same time sparsify the depth maps.

$$\begin{aligned}
&\forall NV_k \in \mathcal{D}_{\text{nerfmentation},s} \subseteq \mathcal{D}_{\text{nerfmentation}}, \\
&\text{mask}_{NV_k}(u, v) = \mathbb{1}\{d_{NV_k,uv} > 0\}, \\
&\text{where} \\
&d_{NV_k,h} = K_C \cdot (R_W^{NV_k} \cdot \text{PC}_s + t_W^{NV_k}), \\
&K_C \in \mathbb{R}^{3 \times 3}, \quad R_W^{NV_k} \in \mathbb{R}^{3 \times 3}, \quad t_W^{NV_k} \in \mathbb{R}^3, \\
&\text{PC}_s \in \mathbb{R}^{N \times 3}.
\end{aligned} \tag{4}$$

where NV_k is the novel view which is defined by the rotation matrix $R_W^{NV_k} \in \mathbb{R}^{3 \times 3}$ and the translation vector $t_W^{NV_k} \in \mathbb{R}^3$. The depth map of novel view NV_k retrieved from the ground-truth point cloud PC_s might have multiple depth values per pixel u, v which is irrelevant in our case since we only need to consider occupancy which is unaffected by multi-occupancy.

For future work, we plan to investigate the impact of this proposed method. Our proposed method sparsifies each RGB-D image again and excludes the sky, a step that is already done during the evaluation on KITTI. As a result, we expect this method to not yield a significant improvement over our proposed vanilla NeRFmentation. However, we do expect substantial benefits for renders captured from extreme poses. Since these renders would deviate strongly from the data distribution of KITTI and would be too sparse for Waymo, we expect a notable performance loss on KITTI and no gain on Waymo. As a result, our extended method

might not be beneficial for current datasets.

Figure F.1 shows rendered RGB-D images from challenging poses and how the occupancy masks can effectively remove these artifacts.

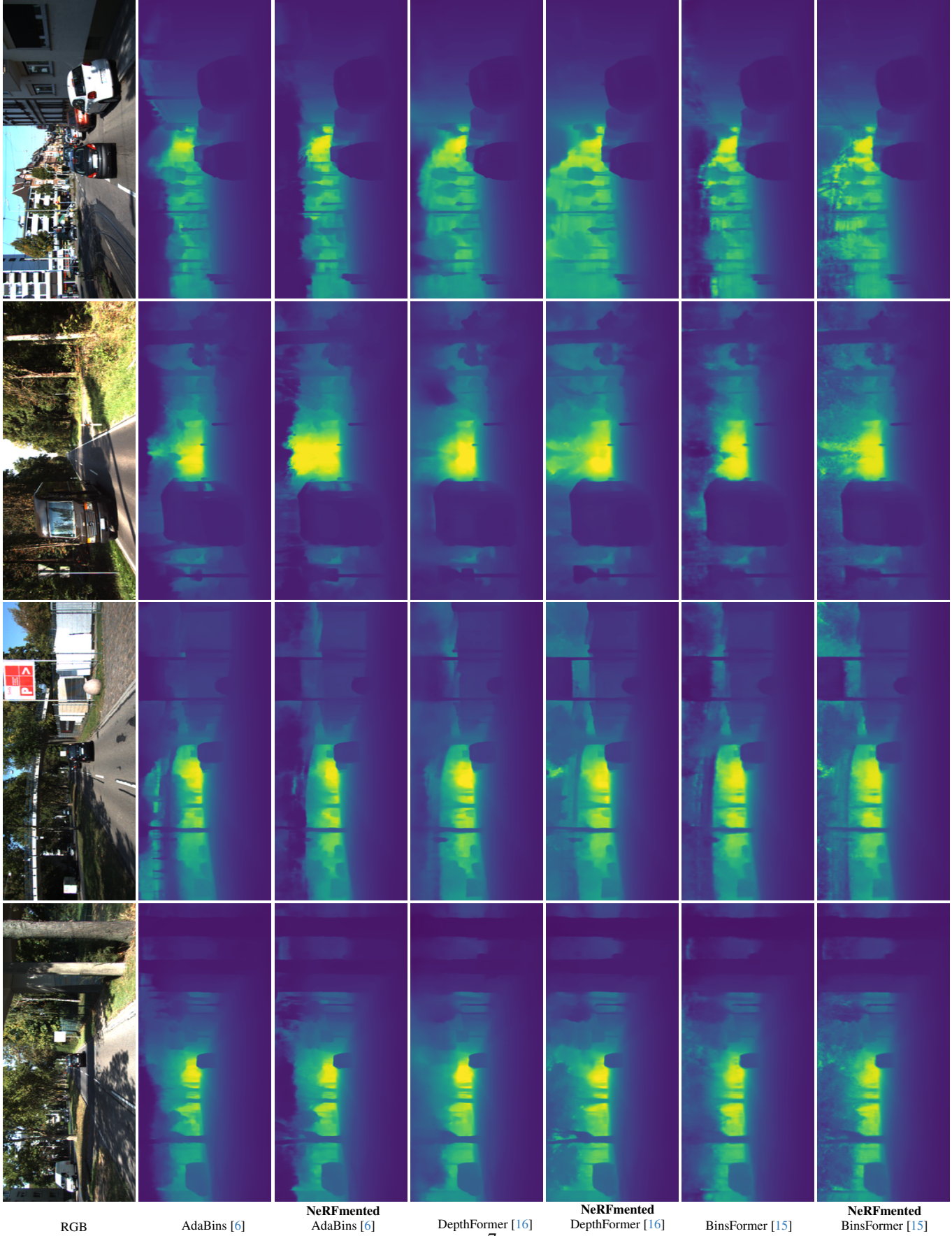


Figure B.1. **Qualitative Results on the KITTI [12] dataset.** We show the performance of NeRFmentation (Ours Interpolated) compared to vanilla-trained AdaBins [6], DepthFormer [16] and BinsFormer [15] leading to improved predictions by using NeRF augmented data for introducing additional viewpoints in the training images. Both the NeRFmented models and vanilla-trained models have been trained on the KITTI Eigen [9, 12] train split and evaluated on test split. Color scale: 0 (purple) to 80 meters (yellow).

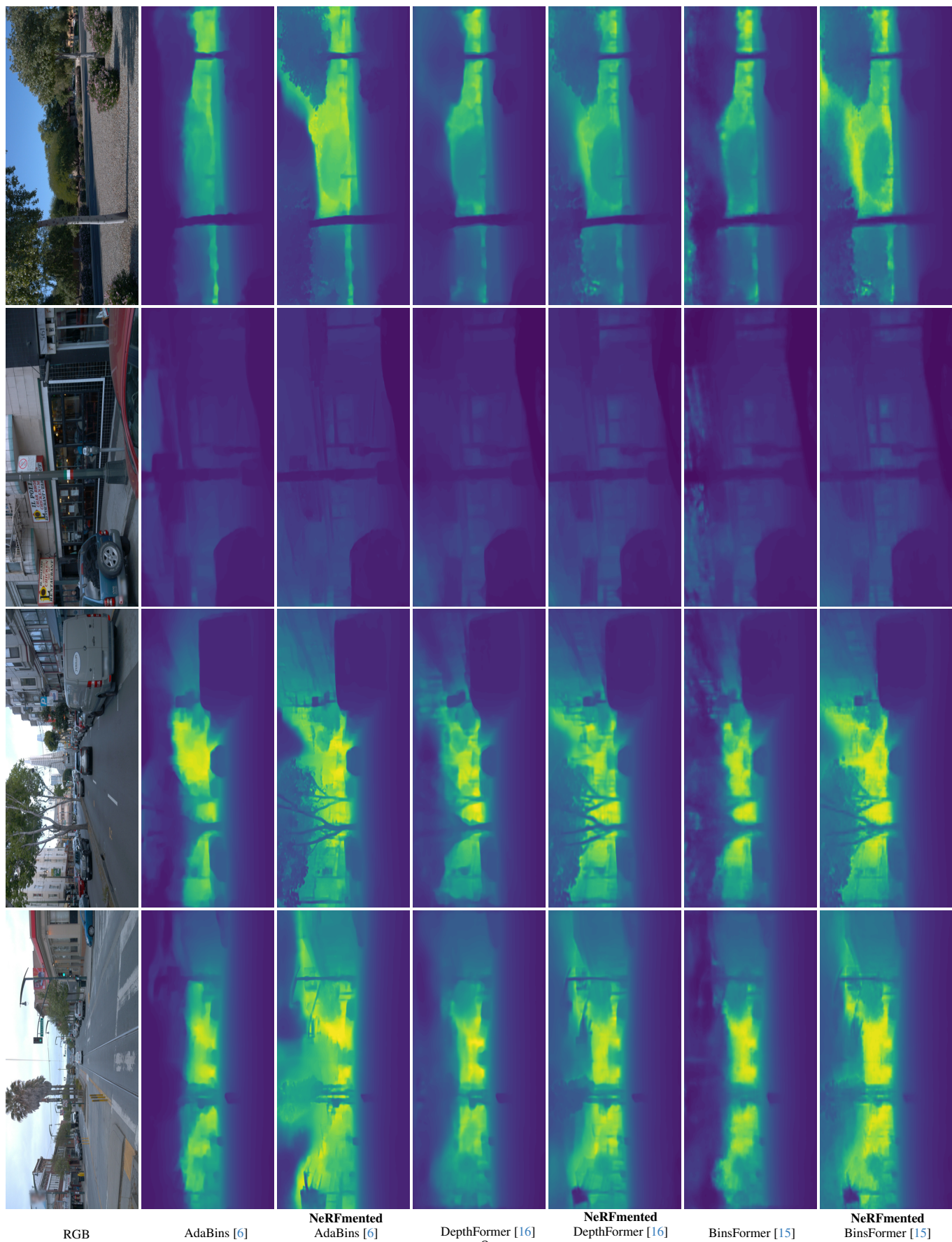


Figure B.2. **Qualitative predictions on the Waymo [35] dataset.** We show the performance of NeRFmentation (Ours) compared to AdaBins [6], DepthFormer [16] and BinsFormer [15]. The color scale goes from 0 (purple) to 80 meters (yellow). Best viewed on a monitor zoomed in.

